- Electronic Supplementary Information (ESI) -

Dissolution of zirconium-cerium oxide solid solution in an aqueous system

Taishi Kobayashi,[1*] Yutaro Sato,[1] Ryutaro Tonna,[1] Daiju Matsumura,[2]

Takayuki Sasaki,[1] and Atsushi Ikeda-Ohno[3*]

[1] Department of Nuclear Engineering, Kyoto University, Kyotodaigaku-katsura,

Nishikyo-ku, Kyoto 615-8540, Japan

[2] Materials Sciences Research Center, Japan Atomic Energy Agency (JAEA), 2-4 Shirakata,

Tokai-mura, Naka-gun, Ibaraki 319-1195, Japan

[3] Advanced Science Research Center, Japan Atomic Energy Agency (JAEA), 2-4 Shirakata,

Tokai-mura, Naka-gun, Ibaraki 319-1195, Japan

* Corresponding authors:

kobayashi@nucleng.kyoto-u.ac.jp (T.K.) and ikeda.atsushi16@jaea.go.jp (A.I.-O.)

Contents

1. **Rietveld refinement for powder X-ray diffraction data**

For detailed investigation of the solid phases of ZC73 (molar Zr/Ce = 7/3) and ZC37 (Zr/Ce = 3/7) before and after immersion, the PXRD patterns were fitted and refined with the Rietveld method using the Rigaku SmartLab Studio II software. The cubic CeO_2 phase (CeO_2(c)) (ICSD No. 28753, $Fm\bar{3}m$) and tetragonal ZrO_2 phase (ZrO_2(t)) (ICSD No. 23928, $P4_2/nmc$) were first assigned as constituents based on the peak positions. Then, the background, lattice parameters, scale factor, peak profiles for CeO_2(c) and ZrO_2(t) were all refined.

Table S1 Crystallographic parameters obtained by Rietveld refinement for PXRD data of ZC73 samples

Sample No.	ZC73-1	ZC73-2	ZC73-4	ZC73_6	ZC73_7
Crystal system			Tetragonal		
Space group			137: $P4_2/nmc$		
a / Å	3.6560(1)	3.65068(14)	3.65164(15)	3.6576(3)	3.6558(4)
c / Å	5.2543(3)	5.2507(3)	5.2516(3)	5.2567(6)	5.2556(7)
Weight-%	82.8(3)	87.94(17)	89.01(13)	43.3(3)	46.9(3)
Crystal system			Cubic		
Space group			225: $Fm\bar{3}m$		
a / Å	5.3469(5)	5.3317(9)	5.3328(6)	5.3846(6)	5.3842(6)
Weight-%	17.2(3)	12.06(17)	10.99(13)	56.7(3)	53.1(3)
R_{wp} (%)	12.24	8.31	7.12	19.09	21.63
R_p (%)	8.45	5.08	4.76	19.10	21.41
S	1.1039	1.4728	1.2295	1.5242	1.7686
χ^2	1.2187	2.169	1.5117	2.3231	3.1278
Sample No.	ZC73_8	ZC73_9	ZC73_10	ZC73_11	ZC73_12
Crystal system			Tetragonal		
Space group			137: $P4_2/nmc$		
a / Å	3.6549(5)	3.6550(3)	3.6629(3)	3.6561(3)	3.65895(17)
c / Å	5.2544(9)	5.2589(6)	5.2644(5)	5.2567(5)	5.2579(3)
Weight-%	41.0(3)	58.12(15)	88.5(3)	85.9(2)	84.7(2)
Crystal system			Cubic		
Space group			225: $Fm\bar{3}m$		
a / Å	5.3847(6)	5.3769(3)	5.3567(9)	5.3512(3)	5.3237(11)
Weight-%	59.0(3)	41.88(15)	11.5(3)	14.1(2)	15.3(2)
R_{wp} (%)	22.15	8.36	17.12	8.76	13.02
R_p (%)	22.21	5.49	13.21	6.00	9.02
S	1.7293	2.0185	1.1983	2.1069	1.1035
χ^2	2.9906	4.0744	1.4359	4.4388	1.2178

Table S2 Crystallographic parameters obtained by Rietveld refinement for PXRD data of ZC37 samples

Sample No.	ZC37-1	ZC37-2	ZC37-4	ZC37_6	ZC37_7
Crystal system			Cubic		
Space group			225: $Fm\bar{3}m$		
a / Å	5.39112(13)	5.3938(4)	5.39638(19)	5.3955(3)	5.39944(19)
Weight-%	85.8(2)	76.3(8)	81.0(6)	75.2(4)	79.7(4)
Crystal system			Tetragonal		
Space group			137: $P4_2/nmc$		
a / Å	3.6899(9)	3.6790(13)	3.6774(10)	3.7118(6)	3.7183(10)
c / Å	5.274(2)	5.281(3)	5.278(2)	5.3359(15)	5.311(3)
Weight-%	14.2(2)	23.7(8)	19.0(6)	24.8(4)	20.3(4)
R_{wp} (%)	20.30	19.87	21.53	13.78	15.64
R_p (%)	18.99	20.89	14.32	13.44	14.78
S	1.4829	1.5736	1.5653	1.0161	1.1489
χ^2	2.1991	2.4763	2.4502	1.0324	1.3199
Sample No.	ZC37_8	ZC37_9	ZC37_10	ZC37_11	ZC37_12
Crystal system			Cubic		
Space group			225: $Fm\bar{3}m$		
a / Å	5.3935(3)	5.3942(5)	5.40194(16)	5.4099(3)	5.4016(2)
Weight-%	68.5(3)	78.7(5)	75.6(3)	80.3(7)	83.1(4)
Crystal system			Tetragonal		
Space group			137: $P4_2/nmc$		
a / Å	3.7245(10)	3.6910(9)	3.6469(6)	3.6694(14)	3.6548(11)
c / Å	5.340(3)	5.321(2)	5.2479(15)	5.267(3)	5.280(2)
Weight-%	31.5(3)	21.3(5)	24.4(3)	19.9(7)	16.9(4)
R_{wp} (%)	11.36	28.03	15.23	21.54	18.60
R_p (%)	10.83	22.79	14.09	22.60	19.91
S	0.8176	2.0298	0.9306	1.0256	0.8319
χ^2	0.6684	4.1201	0.8660	1.0518	0.6921

2. X-ray absorption spectroscopy

2.1. Ce K-edge XANES

As shown in Fig. S1, the absorption edge (first inflection point) of Ce K-edge XANES spectra varies amongst Ce(IV) compounds. However, they are all higher in energy than the absorption edge for Ce(III) (e.g. 40.43 keV for $Ce^{III}_2(SO_4)_3$) and close to the edge position of $Ce^{IV}O_2$. This means that the Ce K-edge XANES spectra given in Figs. S2 and S5 are indicative of the dominant presence of Ce(IV) in the series of the samples.

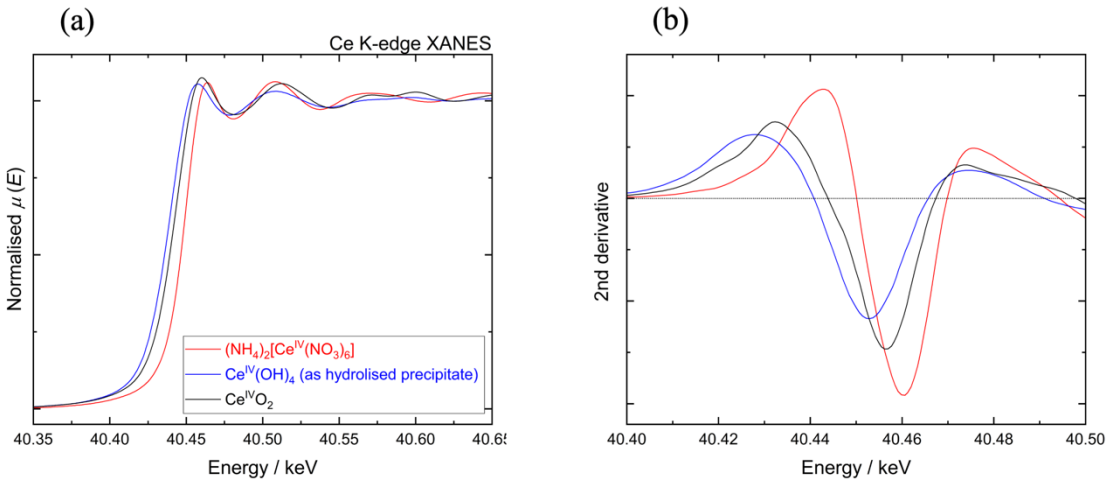

Figure S1. (a) Ce K-edge XANES spectra of different Ce(IV) compounds and (b) the second derivatives of the spectra in (a). The intersections of the second derivatives and the zero-line (dotted line) in (b) indicate the first inflection points (= absorption edge) of the spectra.

2.2. XANES for Zr/Ce = 7/3 (ZC73)

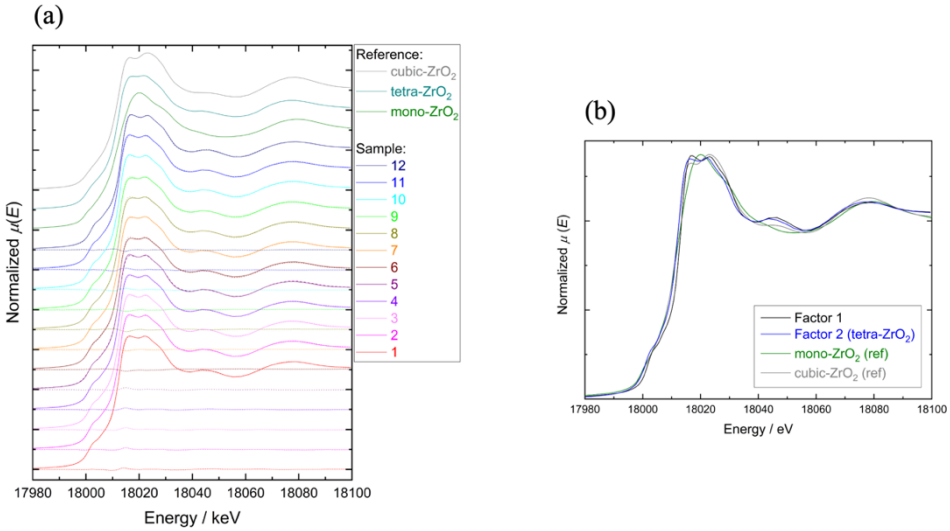

Figure S2. (a) Zr K-edge XANES spectra of 12 samples for Zr/Ce = 7/3 and their reproduction by factor analysis with two principal factors together with three references of mono-, tetra-, and cubic-ZrO_2 (solid lines; experimental data, dash lines; FA-reproduced data, dotted lines; difference between the experimental data and the FA-reproduced data), and (b) the XANES spectra of FA-extracted principal factors. The sample numbers in (a) correspond to the ID numbers in Table 1 in the main text.

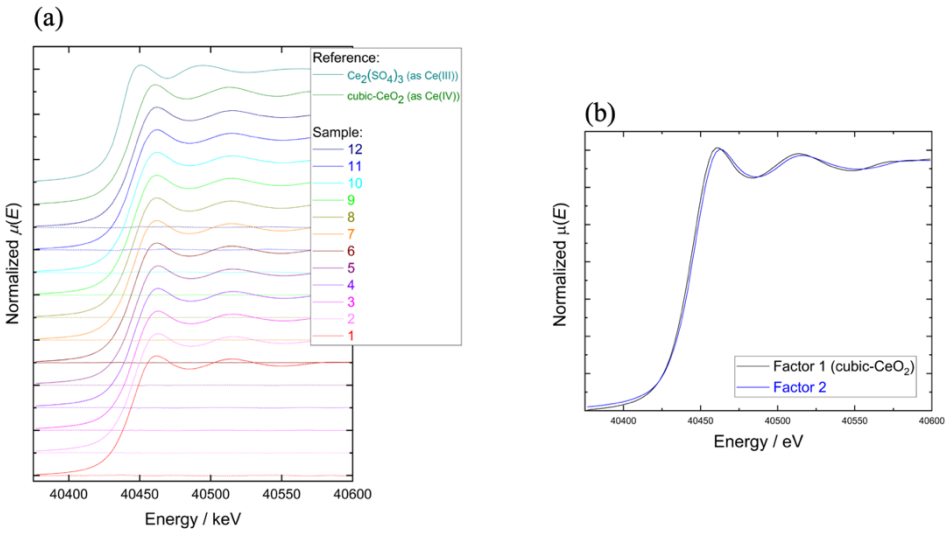

Figure S3. (a) Ce K-edge XANES spectra of 12 samples for Zr/Ce = 7/3 and their reproduction by factor analysis with two principal factors together with two references of cubic-$Ce^{IV}O_2$ and $Ce^{III}_2(SO_4)_3$ (solid lines; experimental data, dash lines; FA-reproduced data, dotted lines; difference between the experimental data and the FA-reproduced data), and (b) the XANES spectra of FA-extracted principal factors. The sample numbers in (a) correspond to the ID numbers in Table 1 in the main text.

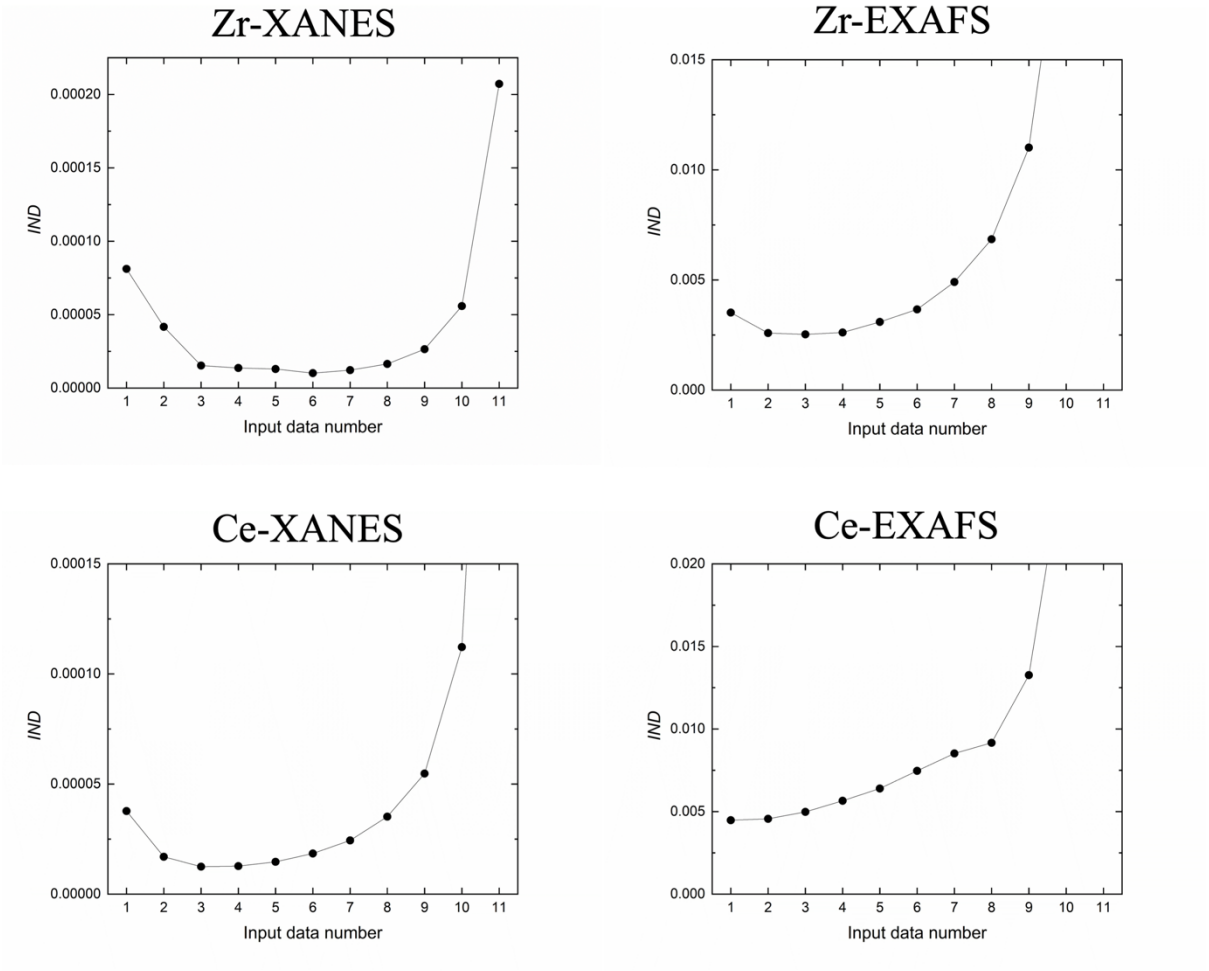

Figure S4. Variation of factor indicator function (IND)[1] for series of XAS spectra for Zr/Ce = 7/3 as an increase in the number of principal factors (input data number).

2.3. XANES for Zr/Ce = 3/7 (ZC37)

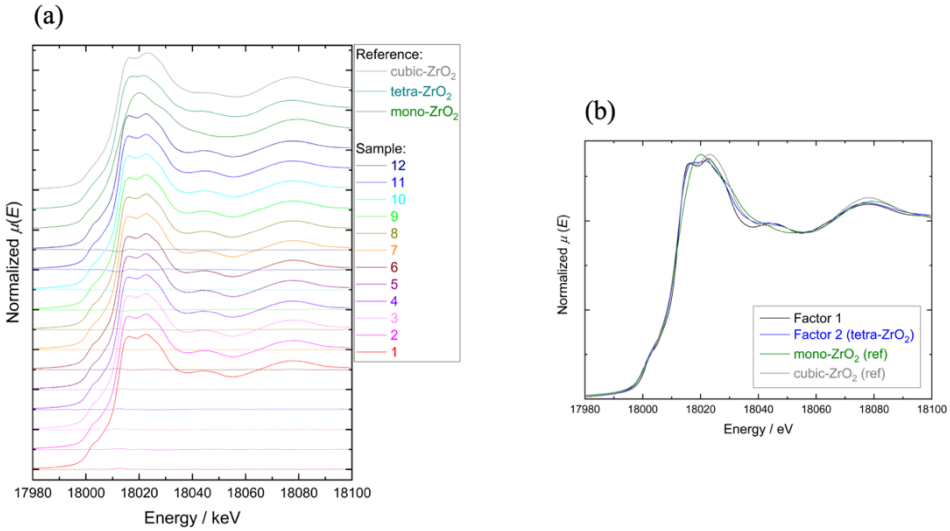

Figure S5. (a) Zr K-edge XANES spectra of 12 samples for Zr/Ce = 3/7 and their reproduction by factor analysis with two principal factors together with three references of mono-, tetra-, and cubic-ZrO_2 (solid lines; experimental data, dash lines; FA-reproduced data, dotted lines; difference between the experimental data and the FA-reproduced data), and (b) the XANES spectra of FA-extracted principal factors. The sample numbers in (a) correspond to the ID numbers in Table 1 in the main text.

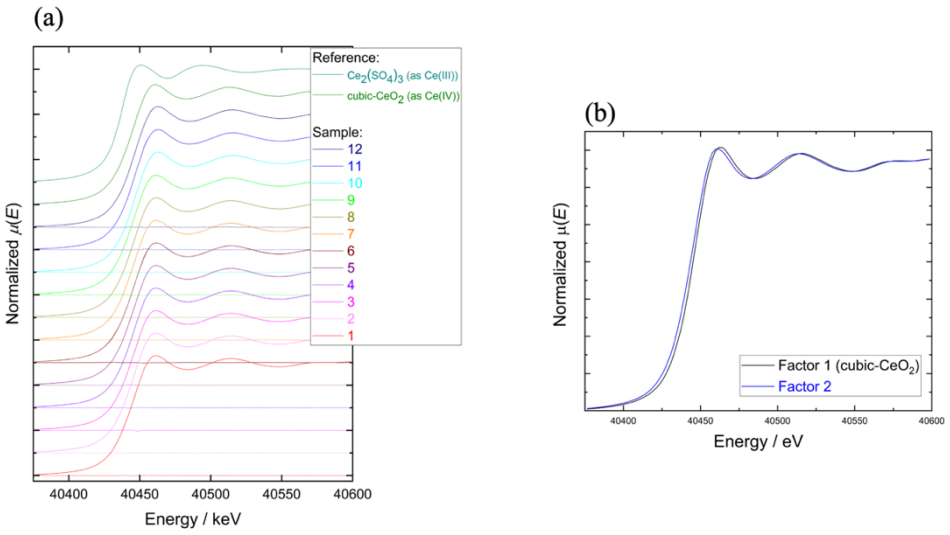

Figure S6. (a) Ce K-edge XANES spectra of 12 samples for Zr/Ce = 3/7 and their reproduction by factor analysis with two principal factors together with two references of cubic-$Ce^{IV}O_2$ and $Ce^{III}_2(SO_4)_3$ (solid lines; experimental data, dash lines; FA-reproduced data, dotted lines; difference between the experimental data and the FA-reproduced data), and (b) the XANES spectra of FA-extracted principal factors. The sample numbers in (a) correspond to the ID numbers in Table 1 in the main text.

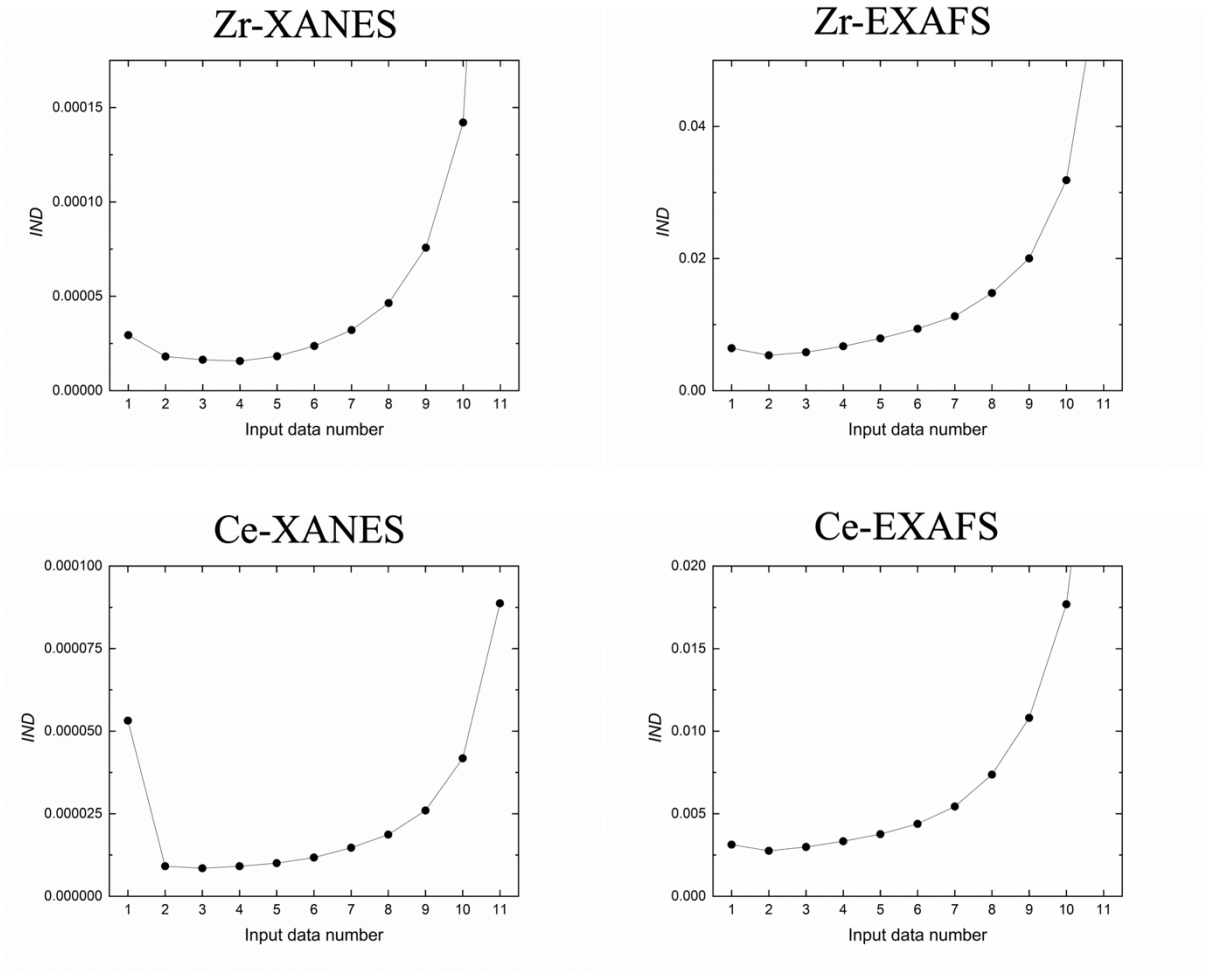

Figure S7. Variation of factor indicator function (IND)[1] for series of XAS spectra for Zr/Ce = 3/7 as an increase in the number of principal factors (input data number).

2.4. Comparison of XANES spectra between Zr/Ce = 7/3 and 3/7 (ZC73 and -37)

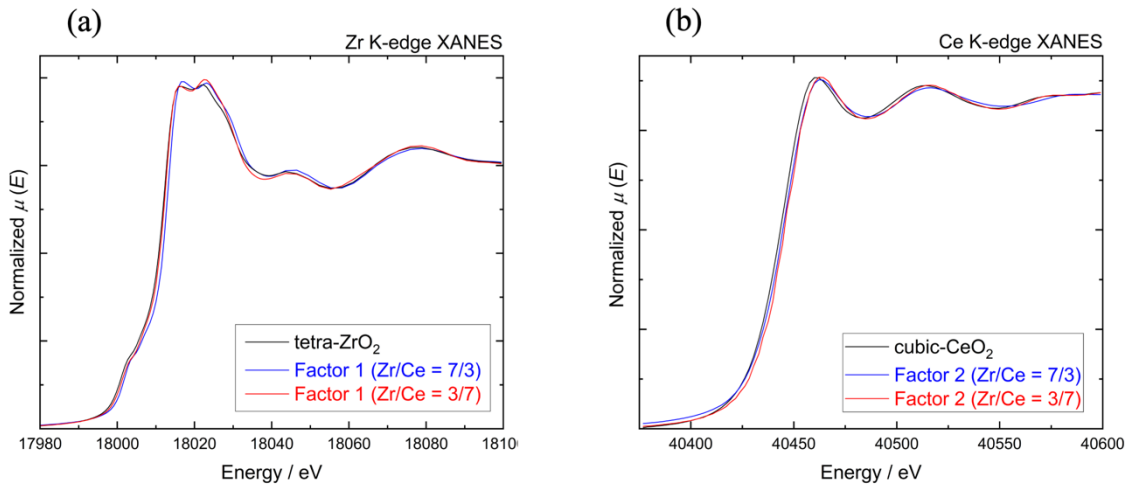

Figure S8. XANES spectral comparison of unidentified factors between Zr/Ce = 7/3 and 3/7 at Zr K-edge (a) and Ce K-edge (b).

3. Scanning electron microscopy

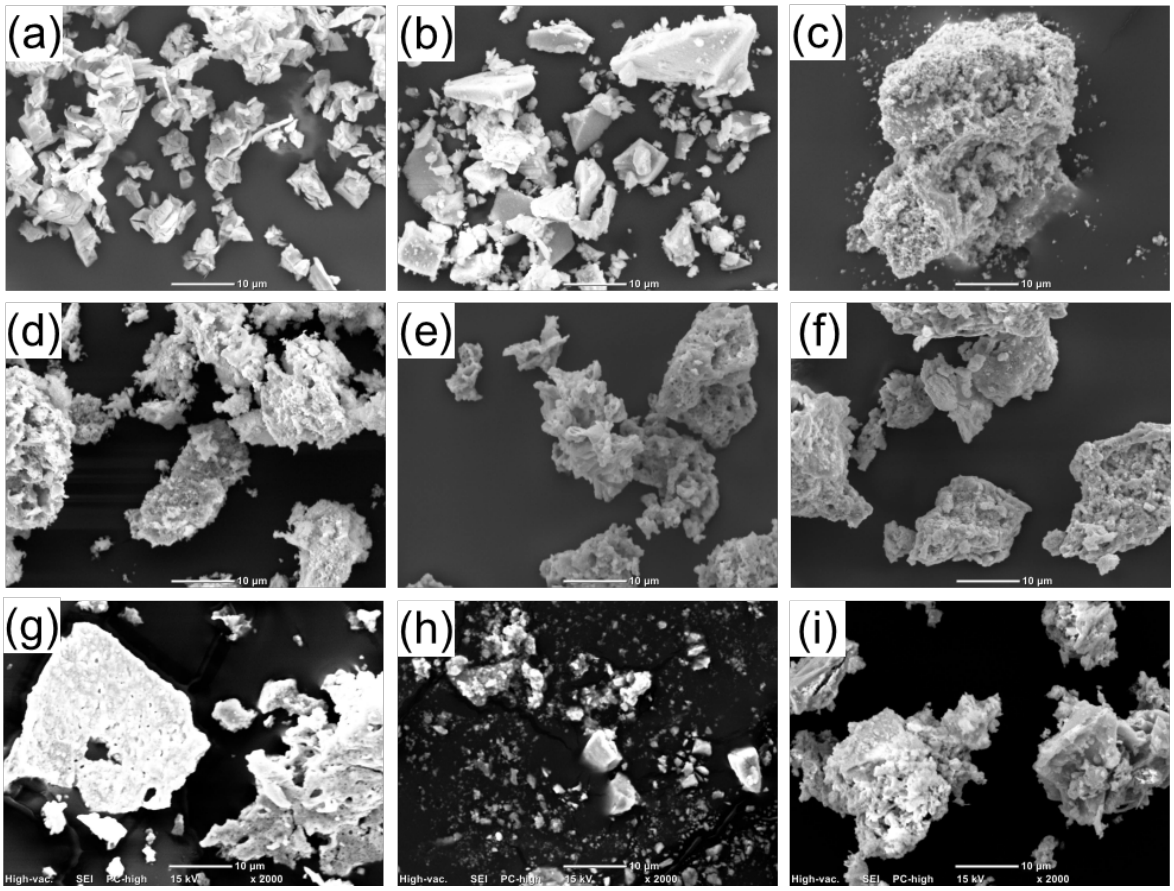

Figure S9. SEM images of (a) CeO_2(c), (b) CeO_2(c) nanopowder, (c) ZCX1, (d) ZC37-1, (e) ZC37-7, (f) ZC37-11, (g) ZC73-1, (h) ZC73-5, and (i) ZC73-7.

4. Pourbaix diagram

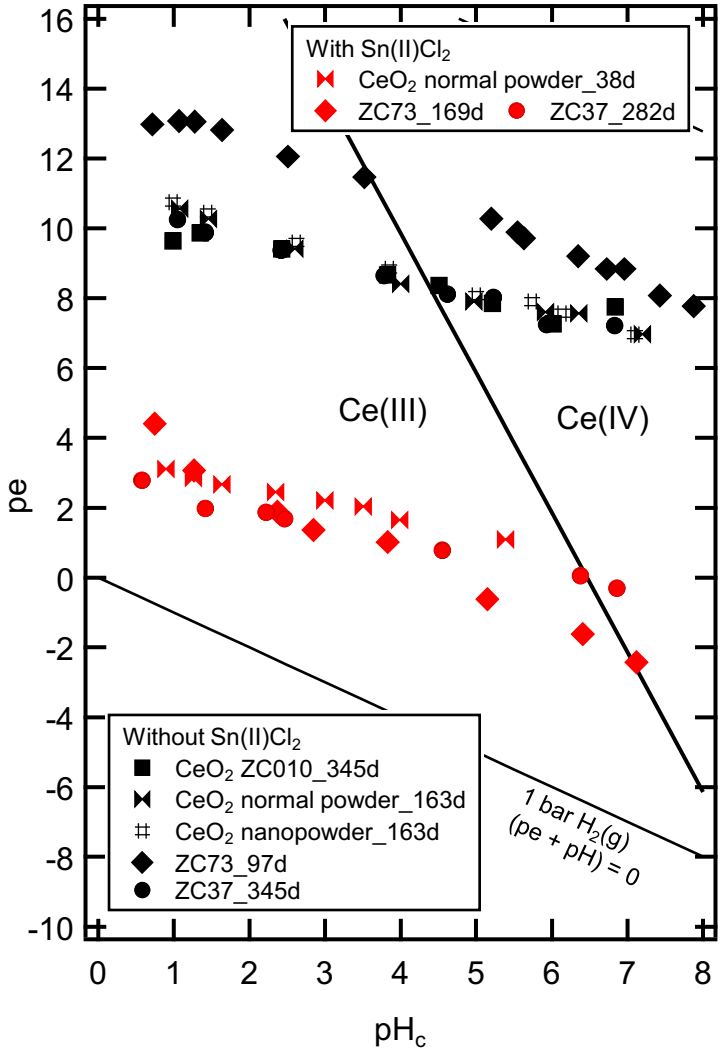

Figure S10. Measured pH and Eh values and the redox equilibrium lines calculated from Ce^{4+}/Ce^{3+} (+1.72 V).[2, 3]

5. Thermodynamical calculation for solubility

The redox reaction between Ce^{4+} and Ce^{3+} can be described as follows with the standard redox potential (+1.72 V),[2, 3]

$$Ce^{4+} + e^{-} \leftrightarrow Ce^{3+} \quad \text{S1.}$$

Based on Eq. S1, the concentration of Ce^{3+} can be calculated using the following equation with a measured Eh value,

$$\log[Ce^{3+}] = \frac{1}{0.059}(Eh - 1.72) + \log[Ce^{4+}] \quad \text{S2.}$$

The hydrolysis reactions of Ce^{4+} and Ce^{3+} are given as follows,

$$Ce^{4+} + nOH^{-} \leftrightarrow Ce(OH)^{4-n} \quad \text{S3,}$$

$$\beta_{4,n} = \frac{[Ce(OH)^{4-n}]}{[Ce^{4+}][OH^{-}]^{n}} \quad \text{S4,}$$

$$Ce^{3+} + mOH^{-} \leftrightarrow Ce(OH)^{3-m} \quad \text{S5,}$$

$$\beta_{3,m} = \frac{[Ce(OH)^{3-m}]}{[Ce^{3+}][OH^{-}]^{m}} \quad \text{S6,}$$

where $\beta_{4,n}$ and $\beta_{3,m}$ are the hydrolysis constants of Ce^{4+} and Ce^{3+}, respectively.

The concentration of Ce^{4+} is limited by the solubility limit of sparingly soluble CeO_2(s) and the solubility product (K_{sp}) is defined as follows,

$$CeO_2(s) + 2H_2O \leftrightarrow Ce^{4+} + 4OH^{-} \quad \text{S7,}$$

$$K_{sp} = [Ce^{4+}][OH^{-}]^{4} \quad \text{S8.}$$

Therefore, the total Ce concentration dissolved in the system ($[Ce]_{tot}$) can be calculated as a function of pH and Eh using Eqs. S2, S4, S6, and S8. From the measured Eh values given in Fig. S10, the Eh values were inter/extrapolated for the whole pH range, and $[Ce]_{tot}$ was calculated based on the reported $\beta_{4,n}$, $\beta_{3,m}$, and K_{sp} values[4-6] summarised in Table S3. The obtained solubility curve is given in Fig. 10 (main text) as a solid line.

For calculating the solubility of Zr, the hydrolysis of Zr^{4+} must be considered, the reaction of which is described as follows,

$$Zr^{4+} + nOH^- \leftrightarrow Zr(OH)^{4-n} \quad \text{S9,}$$

$$\beta_{4,n} = \frac{[Zr(OH)^{4-n}]}{[Zr^{4+}][OH^-]^n} \quad \text{S10,}$$

where $\beta_{4,n}$ is the hydrolysis constants.

The solubility product of ZrO_2(s) is described as follows,

$$ZrO_2(s) + 2H_2O \leftrightarrow Zr^{4+} + 4OH^- \quad \text{S11,}$$

$$K_{sp} = [Zr^{4+}][OH^-]^4 \quad \text{S12.}$$

The total Zr concentration in the system ($[Zr]_{tot}$) can be thus calculated as a function of pH using Eqs. S10 and 12. The hydrolysis constants and solubility product of Zr^{4+}/ZrO_2(s) are summarised in Table S3.

The thermodynamic data for Sn have been comprehensively reviewed by Gamsjäger et al. and the redox reaction of Sn(II) and Sn(IV) has been suggested together with the standard redox potential as follows,[8]

$$Sn^{4+} + 2H_2(g) \leftrightarrow Sn^{2+} + 2H^+ \quad \text{S13,}$$

$$E^{\circ}(Sn^{4+}/Sn^{2+}) = (0.396 \pm 0.011)\text{V} \quad \text{S14.}$$

Table S3. Thermodynamic constants used for calculating the solubility of Ce ($[Ce]_{tot}$) and Zr ($[Zr]_{tot}$)

Reaction		Ce		Zr	
		Value	Ref	Value	Ref
$MO_2(s)+2H_2O \leftrightarrow M^{4+}+4OH^-$	$\log K_{sp}$	−59.3	6	−62.46	9
$M^{4+}+e^- \leftrightarrow M^{3+}$	E_0	1.72	2, 3	-	-
$M^{4+}+OH^- \leftrightarrow M(OH)^{3+}$	$\log \beta_{4,1}$	14.8	5	14.32	10
$M^{4+}+2OH^- \leftrightarrow M(OH)_2^{2+}$	$\log \beta_{4,2}$	28.0	5	< 25.7	7
$M^{4+}+3OH^- \leftrightarrow M(OH)_3^{+}$	$\log \beta_{4,3}$	35.0	5	-	-
$M^{4+}+4OH^- \leftrightarrow M(OH)_4(aq)$	$\log \beta_{4,4}$	42.0	5	< 45.89	7
$Ce^{3+}+OH^- \leftrightarrow Ce(OH)^{2+}$	$\log \beta_{3,1}$	5.59	4	-	-
$Ce^{3+}+2OH^- \leftrightarrow Ce(OH)_2^{+}$	$\log \beta_{3,2}$	10.4	4	-	-
$Ce^{3+}+3OH^- \leftrightarrow Ce(OH)_3(aq)$	$\log \beta_{3,3}$	14.77	4	-	-

6. Hydrolysis of Ce(III)

Trivalent cerium (Ce(III)) is stable in aqueous solutions. It forms hydroxide precipitate at around neutral pH (pH = 7) (Fig. S11). Cerium is still in the trivalent state in the hydroxide precipitate as long as the precipitate is kept in an aqueous solution, even after 12 hours of air exposure (Figs. S12 and S13). However, when the Ce(III) precipitate is dried in the air, cerium is oxidized from trivalent to tetravalent, eventually converting into $Ce^{IV}O_2$ (Figs. S12 and S13). This indicates that the hydroxide species/precipitate of Ce(III) changes into $Ce^{IV}O_2$ upon drying in the air. Ce K-edge X-ray absorption measurements were performed on the beamline BL11XU at SPring-8. The measurement details are described in Ref. 11.

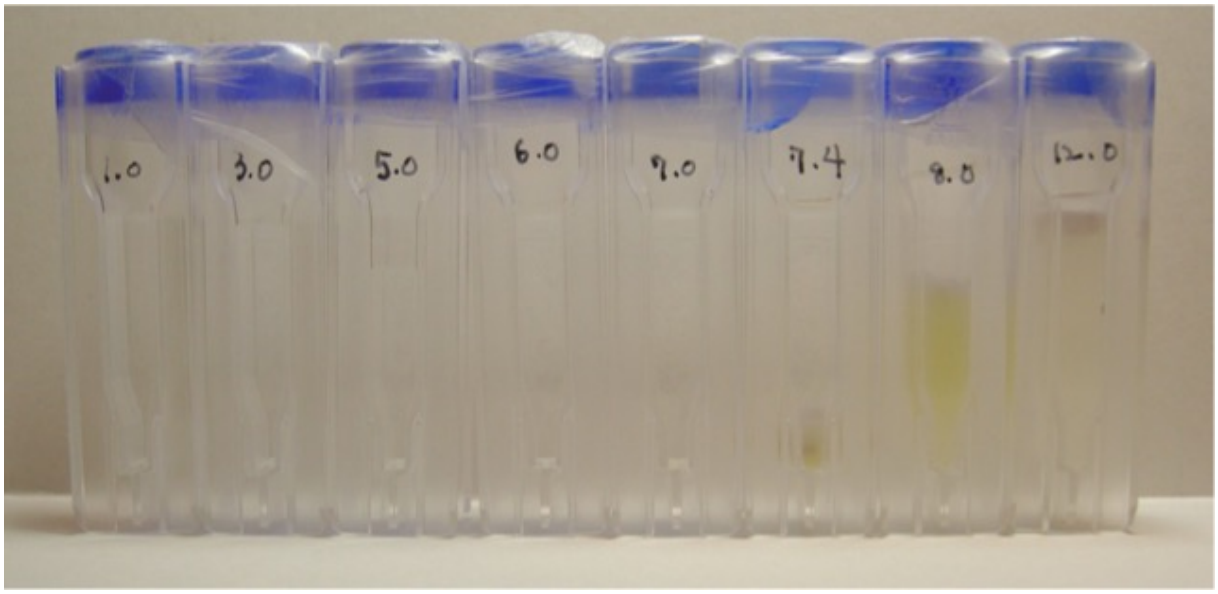

Fig. S11. Appearance of 0.1 M Ce(III) in 0.5 M HNO_3 with different pH values. NaOH was used for pH adjustment.

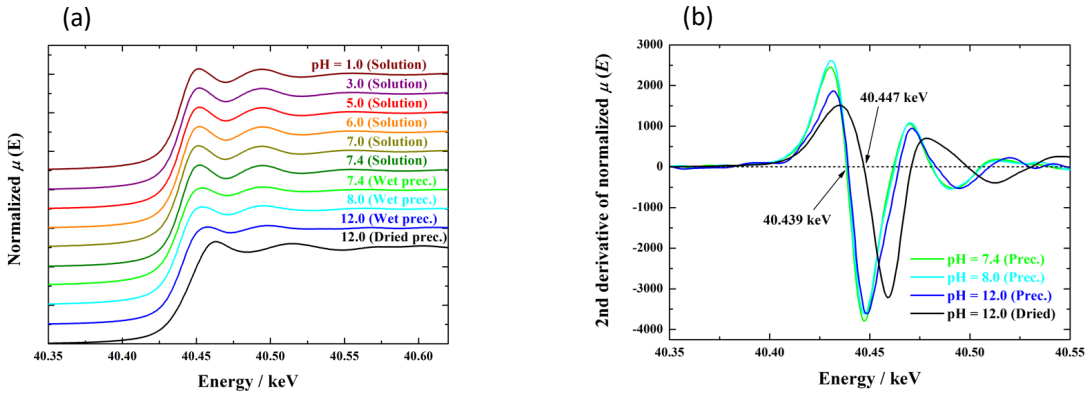

Fig. S12. (a) Ce K-edge XANES spectra of Ce(III) solution/precipitate samples with different pH and (b) their 2nd derivatives (i.e. absorption edge).

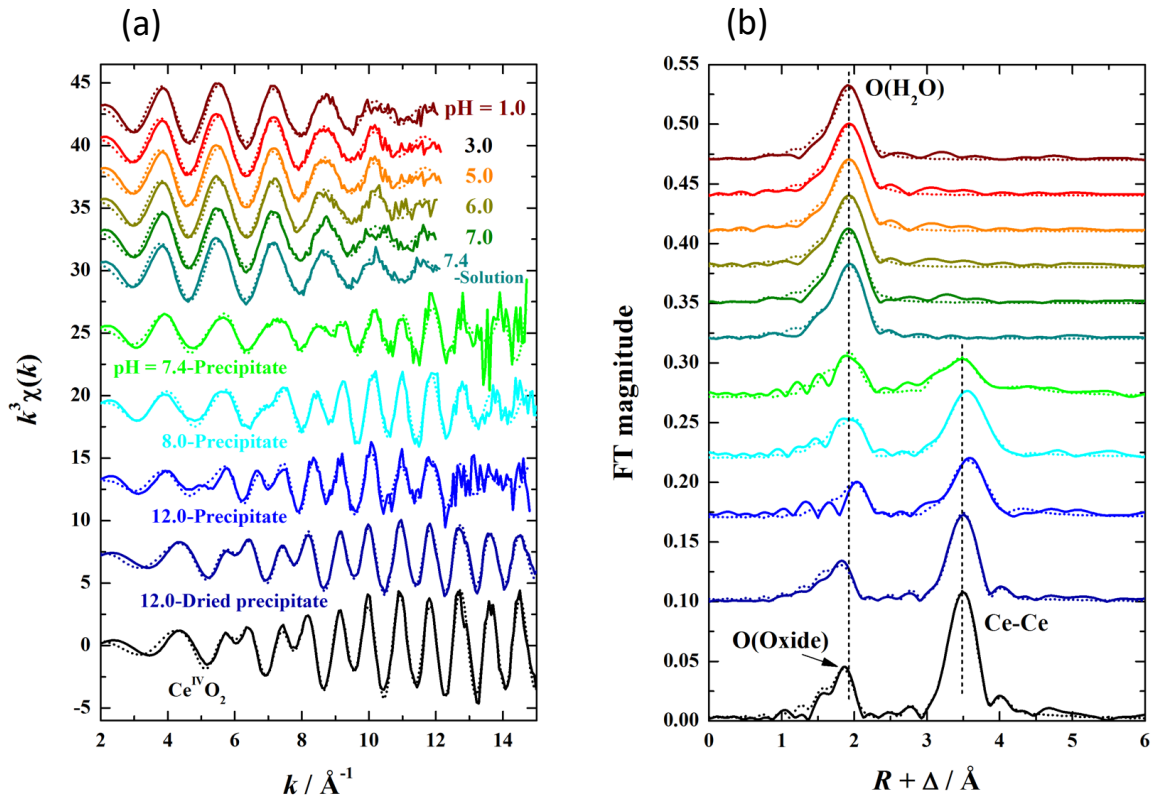

Fig. S13. (a) Ce K-edge EXAFS spectra (k^3-weighted) of Ce(III) solution/precipitate samples with different pH and (b) their corresponding Fourier transforms.

References

1. E. R. Malinowski, *Factor Analysis in Chemistry (3rd edition)*, Wiley-Interscience, New York, 2002.
2. S. G. Bratsch, *Journal of Physical and Chemical Reference Data*, 1989, **18**, 1-21.
3. A. W. Maverick and Q. Yao, *Inorganic Chemistry*, 1993, **32**, 5626-5628.
4. J. H. Lee and R. H. Byrne, *Geochimica Et Cosmochimica Acta*, 1992, **56**, 1127-1137.
5. B. A. Bilal and E. Muller, *Zeitschrift Fur Naturforschung Section a-a Journal of Physical Sciences*, 1992, **47**, 974-984.
6. T. V. Plakhova, A. Y. Romanchuk, S. N. Yakunin, T. Dumas, S. Demir, S. A. Wang, S. G. Minasian, D. K. Shuh, T. Tyliszczak, A. A. Shiryaev, A. V. Egorov, V. K. Ivanov and S. N. Kalmykov, *Journal of Physical Chemistry C*, 2016, **120**, 22615-22626.
7. D. Rai, A. Kitamura, M. Altmaier, K. Rosso, T. Sasaki and T. Kobayashi, *Journal of Solution Chemistry*, 2018, **47**, 855-891.
8. H. Gamsjäger, T. Gajda, J. Sangster, S. K. Saxena and W. Voigt, *Chemical Thermodynamics of Tin*, OECD Publications, Paris, France, 2012.
9. T. Kobayashi, T. Sasaki, I. Takagi and H. Moriyama, *Journal of Nuclear Science and Technology*, 2007, **44**, 90-94.
10. P. Brown, E. Curti, B. Grambow and C. Ekberg, *Chemical Thermodynamics of Zirconium*, North-Holland, Amsterdam, 2005.
11. A. Ikeda-Ohno, C. Hennig, S. Weiss, T. Yaita and G. Bernhard, *Chemistry - A European Journal*, 2013, **19**, 7348-7360.